Carbohydrate Polymers 89 (2012) 1189–1197

Contents lists available at SciVerse ScienceDirect

Carbohydrate Polymers

journal homepage: www.elsevier.com/locate/carbpol

Nanoreinforced bacterial cellulose–montmorillonite composites for biomedical applications

Mazhar Ul-Islam[a], Taous Khan[a,b], Joong Kon Park[a,*]

[a] Department of Chemical Engineering, Kyungpook National University, Daegu 702-701, Republic of Korea
[b] Department of Pharmacy, COMSATS Institute of Information Technology, Abbottabad, Pakistan

ARTICLE INFO

Article history:
Received 5 January 2012
Received in revised form 24 March 2012
Accepted 29 March 2012
Available online 10 April 2012

Keywords:
Bacterial cellulose
Montmorillonite
Nanocomposites
Physico-mechanical properties
Thermal stability

ABSTRACT

Polymer composites containing solid clay nanoparticles have attracted immense attention due to the reinforced physico-mechanical properties of the final product. Bacterial cellulose–montmorillonite (BC–MMT) composites were prepared by impregnation of BC sheets with MMT suspension. FE-SEM showed that MMT adsorbed onto the surface as well as penetrated into the matrix of the BC sheets. Peaks for both BC and MMT were present in the FT-IR spectrum of the composite. XRD also showed diffraction peaks for MMT and BC with a slight decrease in the composite crystallinity from 63.22% of pure BC to 49.68% of BC–MMT3. The mechanical and thermal properties of BC–MMT composites were significantly improved compared to those of the pure BC. Tensile strength for composites was increased up to 210 MPa from 151.3 Mpa (BC) while their degradation temperature extended from 232 °C (BC) up to 310 °C. Similarly, the water holding capacity was decreased while the water release rate was improved for the BC–MMT composites as compared to the pure BC.

1. Introduction

The ever-increasing demand for newer, stronger, stiffer, and lighter materials and structures has led to an extensive research into polymer matrix composites with low specific gravity and high strength and modulus (Gupta, Kumar, Patnaik, & Biswas, 2011). The polymer composites find widespread applications in aircraft, aerospace, automotive, marine, infrastructure, military and sporting goods industries (Andrei, Dima, & Andrei, 2006; Basavarajappa, Arun, & Davim, 2009). Most of these composites are prepared for long term durability using non-degradable polymeric resins and high-strength fibers. However, the environmental impact of persistent non-degradable plastic-based wastes is a global concern. Therefore, various biodegradable polymers have been investigated as replacements for the non-degradable plastics (Gross & Kalra, 2002). In this context, plant-based fibers are renewable, abundant, cheap, lightweight and biodegradable with appropriate mechanical properties (Netravali & Chabba, 2003; Peijs, 2002), due to which they have been used as reinforcing materials in the preparation of various biodegradable polymers (Netravali & Chabba, 2003). However, it is well known that bio-degradable cellulose is associated with non-degradable molecules like lignin and hemicelluloses in plant fibers. The presence of these impurities makes it difficult to develop pure biodegradable polymers with plant fibers in addition to a drastic decrease in the strength of the plant fibers as well as their composites (Bledzki & Gassan, 1999).

In contrast to the plant-based fibers, bacterial cellulose (BC) is a pure cellulose biopolymer produced by certain bacterial strains. It is an exciting biomaterial with unique properties that are superior to those of the plant cellulose, including higher water holding capacity, higher crystallinity, greater tensile strength, an ultrafine fiber network and the ability to be molded into various shapes during production (Li, Kim, Lee, Kee, & Oh, 2011; Ul-Islam, Shah, Ha, & Park, 2011). It is widely used in the food, paper, acoustic, filter membrane, and pharmaceutical industries (Phisalaphong, Suwanmajo, & Sangtherapitiku, 2008) but the most important applications of BC are in the biomedical field, such as wound dressing materials (Czaja, Krystynowicz, Bielecki, & Brown, 2006), artificial skin, vascular grafts, scaffolds for tissue engineering, artificial blood vessels, medical pads and dental implants (Czaja et al., 2006; Li et al., 2011; Ul-Islam et al., 2011). BC constitutes an excellent matrix for the synthesis of functional nanocomposites due to its considerable mechanical properties and biodegradability, in addition to other favorable characteristics. In fact, the mechanical and physical properties of BC can be further reinforced via preparation of composites. Therefore, some researchers have investigated BC reinforced polymer composites with different materials including solid particles of carbonates, iron, aluminum (Serafica, Mormino, & Bungay, 2002), polymers (Ul-Islam et al., 2011), metals (Barud et al., 2011), and conducting materials (Marins et al., 2011).

In recent years, polymer nanocomposites with various clays have been extensively investigated due to their cost effectiveness

* Corresponding author. Tel.: +82 53 950 5621, fax: +82 53 950 6615.
E-mail address: parkjk@knu.ac.kr (J.K. Park).

0144-8617/$ – see front matter © 2012 Elsevier Ltd. All rights reserved.
http://dx.doi.org/10.1016/j.carbpol.2012.03.093

and potential applications in different fields, including the structural, electronics, aerospace, and biomedical industries, and for use in sensors (Akat, Tasdelen, Du Prez, & Yagci, 2008; Liu, Chaudhary, Yusa, & Tade, 2010). Montmorillonite (MMT) is the most widely used clay and has been shown to improve the mechanical properties of composites up to 10-fold (Liu et al., 2010). The composites of MMT and other clay materials with polymers can be synthesized without the use of toxic and expensive organic solvents (Giannelis, Krishnamoorti, & Manias, 1999). The MMT and its products have broad spectrum applications with no side effects in medical fields, such as the cleansing and protection of skin, antibacterial activity (Haydel, Remenih, & Williams, 2008), adsorption of bacteria like *Escherichia coli* and *Staphylococcus aureus*, immobilization of cell toxins (Meng, Zhou, Zhang, & Shen, 2009) and excellent wound healing and blood clotting capabilities (Emami-Razavi et al., 2006).

In the present investigations, BC–MMT composites were synthesized first time through ex situ impregnation with an aim to combine the tremendous properties of BC and MMT to obtain a biomaterial with enhanced physico-mechanical properties for various applications especially in biomedical fields as wound dressing material. These composites are also expected to possess inherited potential antibacterial, wound healing, and drug-carrying properties due to the presence of MMT. The degree of MMT incorporation into the BC sheets in the resulting BC–MMT composites was evaluated by dry weight analysis while the synthesis of the composite was confirmed by FE-SEM, FT-IR and XRD analysis. Properties of the BC–MMT composites, including mechanical strength, thermal stability, water holding capacity (WHC) and water release rate (WRR) were investigated in order to determine their suitability for applications in various fields.

2. Materials and methods

2.1. Microorganism and cell culture

Gluconacetobacter hansenii PJK (KCTC 10505BP) was grown on a basal medium containing glucose 10 g/L, yeast extract 10 g/L, peptone 7 g/L, acetic acid 1.5 mL/L, and succinate 0.2 g/L of distilled water (Ul-Islam et al., 2011). The pH of the medium was adjusted to 5.0 with 1 M NaOH. The prepared basal medium was sterilized for 15 min at 121 °C. Colonies of *G. hansenii* PJK were inoculated into a 50 mL medium in a 250 mL flask shaken at 150 rpm and cultured at 30 °C for 24 h.

2.2. Preparation of BC sheets

BC sheets were prepared in a sterilized rectangular container (30 cm × 30 cm × 3 cm). The basal medium was inoculated with 5% pre-culture and incubated under static conditions at 30 °C for 7 days. BC sheets were treated with 0.3 M NaOH at 121 °C for 15 min in order to disrupt and dissolve the microbial cells. The sheets were then washed thoroughly with distilled water until the pH of the water became neutral. BC sheets were stored in distilled water at 4 °C until further use (Ul-Islam et al., 2011).

2.3. Preparation of BC–MMT composites

BC–MMT composites (BC–MMT1, BC–MMT2 and BC–MMT3) were prepared by treating the BC sheets with 1%, 2% and 4% suspensions of MMT (St. Louis, USA), respectively. MMT suspensions were stirred vigorously for 1 h to obtain homogenous mixtures with the smallest possible particle size. BC sheets were immersed in the MMT suspensions and shaken at 150 rpm for 24 h. The experiments were carried out with 2% MMT suspension at 10, 30 and 50 °C in order to determine the appropriate temperature for maximum MMT penetration into the BC sheets. In all cases, the surface water was removed with filter paper and sheets were freeze-dried at −40 °C for 2 days.

2.4. Dry weight analysis

Dry weight analysis was carried out in order to determine the amount of MMT in the BC–MMT composites under different operating temperatures and MMT concentrations. Long rectangular BC sheets of about 2–3 mm thickness were cut into small pieces of approximately equal wet weights. One set of these pieces was immersed in MMT suspensions for the synthesis of BC–MMT composites under different conditions while another set was directly freeze-dried as pure BC (control). The surface water of the BC–MMT composites was removed and then they were freeze-dried. The dried weights of the pure BC and the BC–MMT composites were measured to find out the weight percent of MMT present in BC–MMT composites. The experiments were repeated several times to confirm the reproducibility.

2.5. FE-SEM analysis

Scanning electron microscopy (SEM) of the freeze-dried BC and BC–MMT composites was performed using a Hitachi S-4800 & EDX-350 (Horiba) FE-SEM (Tokyo, Japan). Samples were fixed onto a brass holder and coated with osmium tetra oxide (OsO_4) by a VD HPC-ISW osmium coater (Tokyo, Japan) prior to FE-SEM observation.

2.6. FT-IR spectroscopy

FT-IR spectra of the dried pure BC and BC–MMT2 were recorded by using a Perkin Elmer FTIR spectrophotometer (Spectrum GX & Autoimage, USA, Spectral range: 4000–400 cm^{-1}; Beam splitter: Ge coated on KBr; Detector: DTGS; resolution: 0.25 cm^{-1} (step selectable)). For analysis, the samples were mixed with KBr (IR grade, Merck, Germany) pellets and processed further to obtain IR data which was transferred to the PC to acquire the spectra.

2.7. X-ray diffraction (XRD) analysis

XRD patterns of the samples were recorded on an X-ray diffractometer (X'Pert-APD PHILIPS, Netherlands) with an X-ray generator (3 kW) and anode (LFF Cu). The radiation was Cu Kα of wavelength 1.54 Å. The X-ray generator tension and current were 40 kV and 30 mA, respectively. The angle of scanning was varied from 5° to 80°. The crystallinity indices of the pure and composite BC were determined from the integrated areas of crystalline and amorphous phases, as reported earlier (Focher et al., 2001).

2.8. Thermal gravimetric analysis (TGA)

TGA of BC and BC–MMT composites was carried out using a thermogravimetric/differential thermal analyzer (Seiko Instruments Inc.). A thermogram for TGA was obtained in the range of 30–800 °C, under nitrogen atmosphere with a temperature increase of 10 °C min^{-1}.

2.9. Mechanical properties

The tensile properties of the BC and BC–MMT composites were measured using an Instron Universal Testing Machine (Model 4465, USA) according to the procedure of the American Society for Testing and Materials (ASTM D 882) (Shehzad, Khan, Khan, & Park, 2010). Two metal clamps were placed at either end of each 100 mm × 10 mm rectangular strip of dried sample. The clamps

were then mounted on an Instron 4465 that measured both elongation and maximum tensile load before fracture. The experiment was repeated several times and average values were taken.

2.10. Water holding capacity and water retention rate

The WHC for various samples was measured by the sieve shaking method. Sheets of pure BC and BC–MMT composites were placed in water for complete swelling. These samples were then taken out of the storage container using tweezers, put in a sieve, and shaken twice to remove the surface water followed by weighing immediately. These samples were dried at ambient temperature for 90 h and their weights were measured at different time intervals. Samples were finally dried for 24 h at 50 °C in order to completely remove the water. The WHC of different samples were calculated by using the following formula (Shezad, Khan, Khan, & Park, 2010):

$$\text{Water holding capacity} = \frac{\text{Mass of water removed during drying (g)}}{\text{Dry weight of BC sample (g)}}$$

For determining the WRR, the wet weights of BC and BC–MMT composites were measured, followed by continuously weighing the samples stored under ambient conditions at different time intervals until a constant weight was obtained. The weights of the samples at different time intervals were plotted against time (Shezad et al., 2010).

3. Results and discussion

3.1. Effect of temperature and concentration on the MMT transfer into BC

It is well known that the polyglucosan chains of BC are surrounded by layers of water molecules resulting in a soft gel (Seves et al., 2001). The gel after freeze drying has a spongy appearance with numerous pores of different sizes on the surface and in the matrix of the BC. This porous structure of BC acts as a scaffold to adsorb and absorb various substances present in a solution and in suspension form. The BC–MMT composites were synthesized based on the porous structure of BC and the nano size of the MMT particles. The attachment of MMT nanoparticles onto the surfaces of BC sheets and their penetration into the empty spaces or pores of the BC matrix results in an increase in dry weight of the composites. The presence of the MMT particles on the surface and inside the matrix of BC sheets can be visualized in the SEM micrographs shown in Fig. 1. The relative increase in dry weight of the composites compared to the pure BC indicates the amount of MMT adsorbed. Moreover, the experimental conditions (operating temperature and MMT concentration) for the adsorption of the maximum amount of MMT in the BC–MMT composites were also evaluated on the basis of the dry weight analysis.

To investigate the effect of temperature, the BC was treated with 2% MMT suspension for 24 h at 10, 30 and 50 °C. The results for the dry weights of the BC–MMT composites at different temperatures are shown in Fig. 2, which indicates an increasing trend with increasing temperature up to 50 °C. 20.9% of MMT was adsorbed by the BC–MMT composite at 10 °C. A drastic increase in the amount of adsorbed MMT was observed with an increase in temperature to 30 °C, in which case it was found to be 34.38% of the total composite dry weight. However, a relatively smaller increase occurred in the amount of adsorbed MMT with a further increase in temperature. The final composite contained 40.36% of MMT dry weight at 50 °C. The increase in MMT adsorption at higher temperature may be due to the fact that the MMT suspension is more homogeneous and thinner at higher temperature, causing a better dispersion of MMT particles and efficient penetration into the BC matrix than at lower temperature. The effect of a further increase in temperature was not studied because there was only a modest increase in the dry weight of BC–MMT composites with an increase in temperature from 30 to 50 °C. Moreover, some physical deterioration of BC sheets may also occur at high temperature, especially in the presence of a shear stress generated by a rotation speed of 150 rpm. The temperature of 50 °C was also found to be appropriate for the adsorption of chitosan (Ch) in our previous studies on the BC–Ch composite (Ul-Islam et al., 2011).

The concentration of the MMT suspension can also affect the amount of MMT adsorbed onto the surface and inside the BC sheets. Theoretically, the higher the concentration of the MMT suspension, the greater will be the number of particles penetrating into the BC matrix. However, a very high concentration of MMT can result in the agglomeration of particles, which can adversely affect the composite properties (Olalekan et al., 2010). The effect of the concentration of MMT was evaluated for the preparation of BC–MMT composites using 1, 2 and 4% MMT suspensions. The results shown in Fig. 2 indicated that the amount of MMT adsorbed by the BC–MMT composites increases with increasing MMT concentration. However, the effect was more prominent for MMT concentrations of up to 2%. The amount of adsorbed MMT in BC–MMT1 was 25.72%, which increased to 40.36% in BC–MMT2 and further increased to 45.06% in BC–MMT3. The percentage weight of adsorbed MMT in BC–MMT composites did not increase significantly with an increase in MMT concentration from 2 to 4%. Thus a 2% MMT concentration was sufficient for the saturation of the surface and matrix of BC sheets with MMT particles as shown in SEM micrographs (Fig. 1).

3.2. Morphological characteristics of the BC–MMT composites

A morphological study of the pure BC and the BC–MMT composites was undertaken using FE-SEM in order to confirm the synthesis of BC–MMT composites by assessing the attachment of MMT particles onto the surface and their penetration into the matrix of BC sheets. Moreover, the effects of MMT concentration on these parameters and the overall morphological characteristics were also studied. The SEM micrographs of the pure BC and the BC–MMT composites illustrate a three dimensional arrangement of the micro-fibrils (Fig. 1). The micro-fibrils are randomly arranged in pure BC, which result in the formation of pores with different sizes on the surface and in the entire matrix of the BC sheets (Fig. 1A and B). The small-sized MMT particles can penetrate inside the BC sheets through these pores. Fig. 1 shows that the surfaces of the composites are occupied with MMT particles as compared to the bare surface of the pure BC. The number of MMT particles attached to the surfaces of the BC increases with the increasing concentration of MMT, which can be clearly seen in Fig. 1C, E, and G. The images with higher magnifications revealed an abundance of empty spaces between the fibrils in BC–MMT1, which were considerably decreased in BC–MMT2 and almost completely filled in BC–MMT3 due to the increasing accumulation of MMT particles.

The SEM micrographs of the cross sections of BC and BC–MMT composites, shown in Fig. 1B, D, F, and H, provide further details of the composite structures. The particles that penetrated into the BC sheet have filled the empty space in the entire matrix. The density of MMT particles penetrated and accumulated in the matrices of the composites were increased with increasing MMT concentration, as can be clearly seen in Fig. 1D, F, and H. The empty spaces between the fibrils are almost completely filled in the case of the BC–MMT3. Furthermore, the size of the MMT particles seems to be larger in BC–MMT3, which may be due to the agglomeration of particles in the matrix as reported previously (Olalekan et al., 2010).

The penetration of MMT particles into the BC sheets results in the increased dry weight of the composite, which is also supported

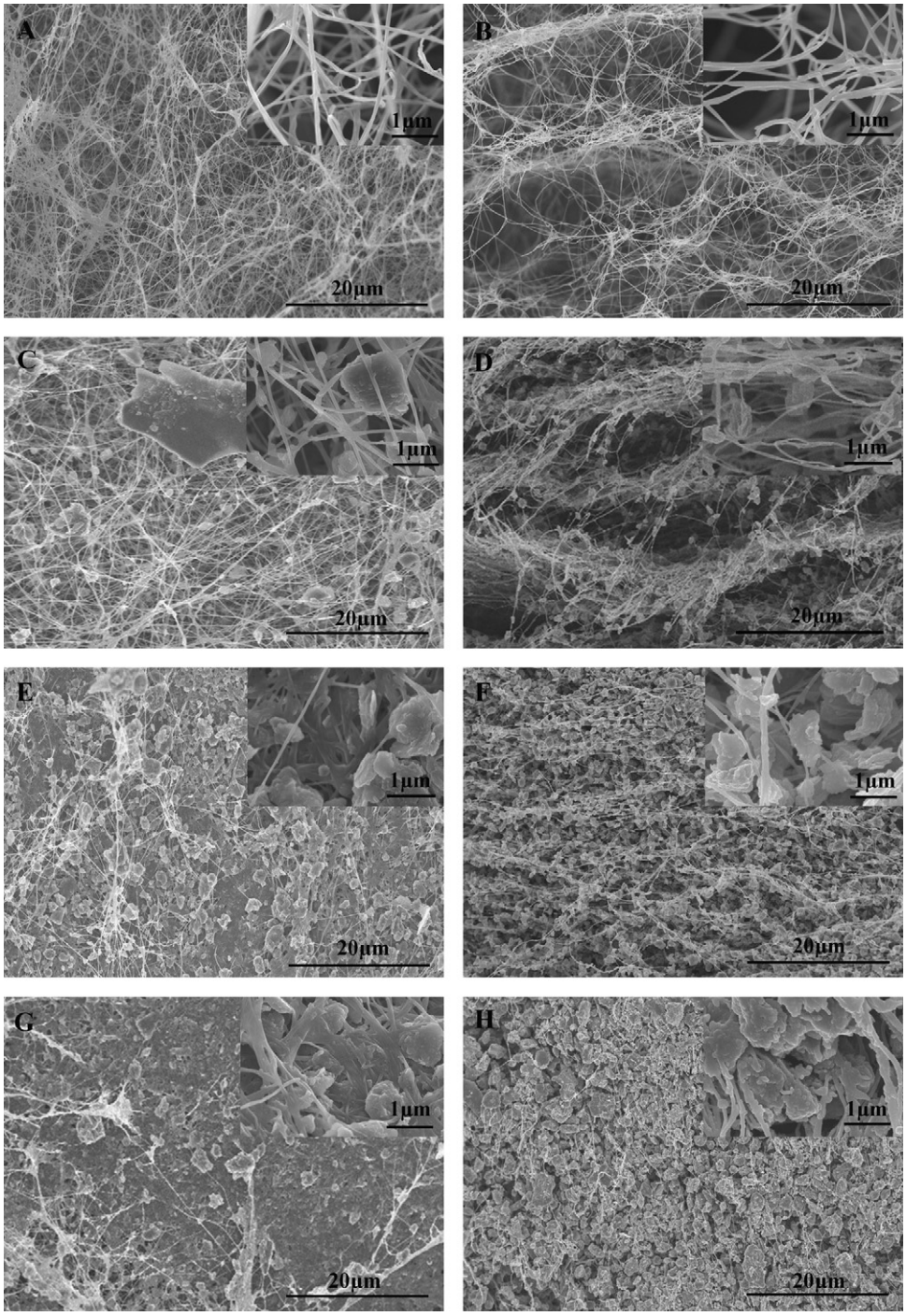

Fig. 1. FE-SEM micrographs of the surface and cross section morphology of the (A, B) pure BC; (C, D) BC–MMT1; (E, F) BC–MMT2; and (G, H) BC–MMT3. The BC–MMT composites (BC–MMT1, BC–MMT2 and BC–MMT3) were prepared by impregnation of BC sheets in respective concentrations (1, 2 and 4%) of MMT suspensions at 150 rpm for 24 h.

by the SEM images displayed in Fig. 1. The presence of hydroxyl groups in both MMT and BC can lead to weak organic–inorganic hydrogen bonding interactions (Darder, Colilla, & Ruiz-Hitzky, 2003; Li, Jia, Zhu, Ma, & Sun, 2010; Theng, 1970). Although the interaction between the individual polymer chain and the clay particles is weak, the total energy adsorbed is high due to the numerous points of interaction (Theng, 1970). These interactions of MMT particles with BC chains, as well as their attachments to the BC surface and penetration inside the BC matrix, can affect the physico-mechanical properties of BC.

3.3. FT-IR analysis

FT-IR spectroscopy is an important tool to determine the functional groups and nature of chemical bonds in a molecule (Ul-Islam et al., 2011). FT-IR analyses of the pure BC and the BC–MMT composites were carried out in order to verify the preparation of the BC–MMT composites by analyzing the specific peak positions. Moreover, the possible hydrogen bonding interaction between the OH groups of BC and MMT can also be investigated using the FT-IR spectra. The IR spectra for pure BC, MMT, and BC–MMT2 are shown

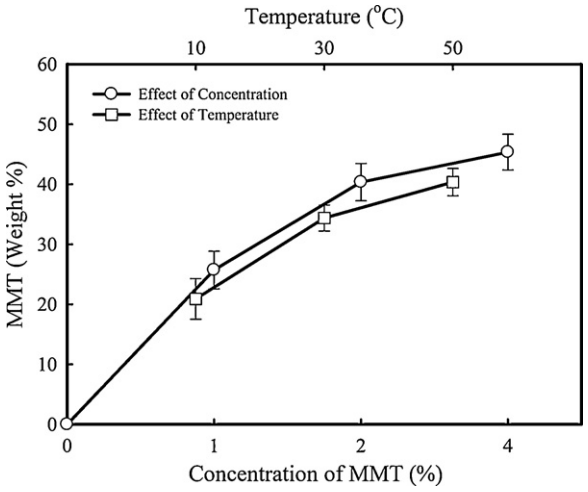

Fig. 2. Effect of the concentration of MMT (at 50 °C) and operating temperature (at 2% MMT concentration) on the amount of MMT incorporated into the BC–MMT composites prepared by impregnation of BC sheets in MMT suspensions at 150 rpm for 24 h.

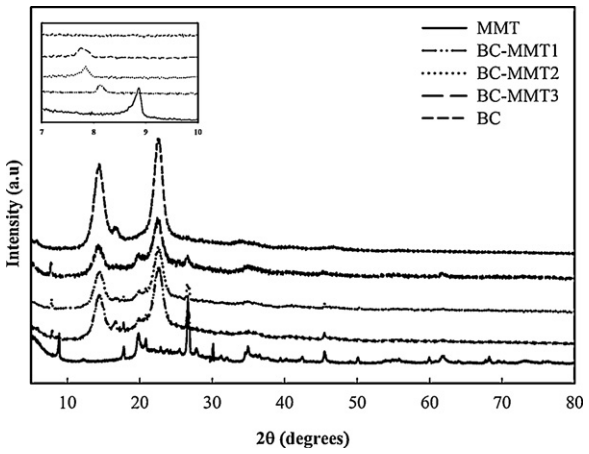

Fig. 4. XRD patterns of pure BC, pure MMT, BC–MMT1, BC–MMT2 and BC–MMT3. The BC–MMT composites (BC–MMT1, BC–MMT2 and BC–MMT3) were prepared by impregnation of BC sheets in respective concentrations (1, 2 and 4%) of MMT suspensions at 150 rpm for 24 h. The smaller angle (7–10°) XRD patterns for all these samples have been shown in the upper left corner.

in Fig. 3, which indicates the peak positions for various functional groups in these samples.

The IR spectrum of pure BC shows characteristic bands at about ~3444 cm^{-1} and 2896 cm^{-1} for stretching vibrations of O—H and C—H, respectively. The presence of the CH group was further supported by its bending vibration at ~1424 cm^{-1}. Other important peaks that appeared at around 1000 cm^{-1} are due to the C—O—C stretching vibration (Shah, Ha, & Park, 2010). The most prominent bands in the IR spectrum of MMT can be found in the region from 3400 to 3700 cm^{-1}. This spectrum showed a sharp peak at 3612 cm^{-1} due to OH stretching and another broad peak centered at 3452 cm^{-1} due to interlayer O—H stretching (hydrogen bonding) arising from Al, Mg (OH) groups of the MMT (Gunister, Pestreli, Unlu, Atici, & Gungor, 2007; Theng, 1970). The adsorbed water molecules in the samples displayed an H—O—H bending vibration at about 1600 cm^{-1} (Gunister et al., 2007). Furthermore, the fingerprint region showed peaks arising from the Si—O stretching and bending at ~1087 and 526 cm^{-1}, respectively. The bending vibration peaks for Mg—O appeared at ~792 cm^{-1} (Gunister et al., 2007).

The IR spectrum of the BC–MMT composite showed the presence of characteristic peaks both from the BC and MMT. The OH peak of pure MMT at 3619 cm^{-1} is present while the broad band near the same region (3432 cm^{-1}) arises due to the merging of peaks for the hydrogen bonding of both BC and MMT. The increase in the hydrogen bonding interactions can be clearly seen although the peak shifts slightly towards lower values. The most evident peak in the BC–MMT spectrum was due to the aliphatic C—H stretching vibration of BC which appeared at 2908 cm^{-1}. A broad band appearing at ~1097 cm^{-1} was due to merging of the bands of C—O—C and Si/Mg—O in BC and MMT, respectively. All the bands in the fingerprint region can be seen in the spectrum of the BC–MMT composite. In a nutshell, the FT-IR spectra give clear evidence of the formation of the BC–MMT composites. Furthermore, they also displayed the hydrogen bonding interaction between the OH moieties of the constituent materials in the composite.

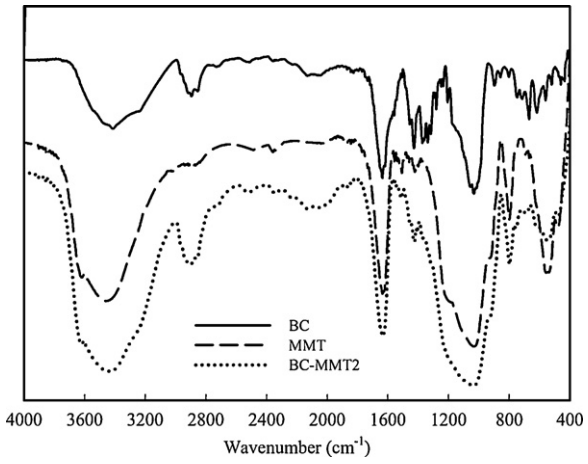

Fig. 3. FT-IR spectral analysis of pure MMT, Pure BC and BC–MMT2. The BC–MMT2 was prepared by impregnation of BC sheets in 2% MMT suspensions at 150 rpm for 24 h.

3.4. X-ray diffraction (XRD) analysis

XRD is most commonly used to investigate the structural features of nanocomposites due to its easiness and availability. XRD is used to evaluate the crystalline structure, the ratio of crystalline to non-crystalline (amorphous) regions, crystal size, the arrangement pattern of crystals and the distance between the planes of the crystal (Pavlidou, 2008). This means that structural changes induced in a crystalline material by blending with other materials can be monitored using the XRD technique. In the present study, XRD analyses were carried out in order to investigate the micro-structural changes in the BC sheets caused by the adsorption and penetration of MMT particles. The XRD patterns of BC, MMT, BC–MMT1, BC–MMT2 and BC–MMT3 are shown in Fig. 4.

The XRD spectrum of the pure BC sheets showed three distinct peaks which appeared at 2θ 14.2°, 16.6°, and 22.4°. These diffraction peaks correspond to the crystallographic planes of (1 1 $\bar{0}$), (1 1 0) and (2 0 0), respectively (Castro et al., 2011). An amorphous halo is also present at 2θ 19.6° representing the amorphous part of the BC. The crystallinity of the pure BC and BC–MMTs composite can be calculated from the integrated areas of crystalline and amorphous region (Focher et al., 2001). The relative crystallinity of the pure BC was 63.22%, which decreased to 55.99, 52.47 and 49.68% in BC–MMT1, BC–MMT2 and BC–MMT3, respectively. This trend is in accordance with previous studies which showed that additives usually decrease the polymer crystallinity (Phisalaphong et al., 2008; Ul-Islam et al., 2011). The penetration and interaction of MMT particles slightly disturb the native hydrogen bonding interactions in BC microcrystalline chains and eventually result in a

lower crystallinity of the composites (Ul-Islam et al., 2011). Various diffraction peaks at 2θ angles of ~8.5°, 17.74°, 26.52°, and 45.52° can be found in the XRD spectra of pure MMT. The major diffraction peaks for both BC and MMT can be observed in the spectrum of the BC–MMT composites, which clearly indicates the formation of the composite and supports the FE-SEM and FT-IR structural confirmations. There is a slight shift towards lower angles in the peak positions in the BC–MMT composite, which may be due to the interaction and interpenetration of the BC chains and MMT layers in a similar way to that reported previously for polystyrene organo clay composites (Pavlidou, 2008; Ray & Okamoto, 2003). A prominent peak corresponding to clay material is usually found in the lower angle region, i.e., below 10° (Gunister et al., 2007; Pavlidou, 2008; Ray & Okamoto, 2003). Pure MMT gives a peak in the region of 8–9° which represents the interlayer distance between the silicate sheets of MMT particles (Gunister et al., 2007). This peak is present in all the BC–MMT composites at a slightly lower position with high FWHM (full width at half maximum) values and decreased intensity. This probably suggests the partial delamination of the interplanar layers of clay particles. Fig. 4 (small angle) shows an expanded and clear picture of such peak shifting. The clay particles form a layered structure. The interaction of these layers with the BC glucose chains and slight penetration of the glucose chains into these layers of clay cause the peak to shift towards a slightly lower angle (Pavlidou, 2008). The peak shifting towards lower angle is slightly increased with higher MMT concentration in the composites. The similar trend was reported for various polymer/clay nanocomposites (Akat et al., 2008; Yu, Zhang & Fu, 2004). As shown in Fig. 4, a slight increase in peak intensity could be found with MMT content in the composites. This might be caused by the agglomeration of MMT in the composite as reported previously for the polymer/clay nanocomposites (Akat et al., 2008).

3.5. Thermogravimetric analysis (TGA)

The thermal stability of nanocomposites is an important factor for their commercial application especially at higher temperatures (Lin & Burggraaf, 1991). The thermal behavior of the pure BC and the BC–MMT composites were investigated using TGA analysis. The TGA curves are shown in Fig. 5. The thermal degradation of BC involves dehydration, depolymerization, and decomposition of glycosyl units followed by the formation of a charred residue (George, Ramana, Bawa, & Siddaramaiah, 2011). Two major weight loss zones can be observed in all these curves. About 8–9% weight loss for pure BC occurred at a temperature range of 80–120 °C. On the other hand, the BC–MMT composites showed only about 5% weight loss in the same temperature range. The weight loss occurring at 80–120 °C is due to the loss of moisture content and interlayer coordinated water molecules (Darder et al., 2003; Khan & Park, 2008; Li et al., 2010). The relatively higher weight loss for the pure BC at this temperature range may be due to its higher WHC as compared to the BC–MMT composites as shown in Table 1. The second phase of degradation starts above 225 °C in all samples. This phase occurs due to the degradation of the main cellulose skeleton (Darder et al., 2003; Li et al., 2010). The maximum weight loss was recorded for all samples during this phase. The weight loss for the pure BC is about 65% during this phase (Fig. 5), which indicates the degradation of the main skeleton of cellulose (Darder et al., 2003; Li et al., 2010). The weight loss during this phase was lower for all the BC–MMT composites than it was for the pure BC. Moreover, the weight loss decreased with increasing concentration of MMT in the composite, and was found to be about 32, 25 and 22% for BC–MMT1, BC–MMT2, and BC–MMT3, respectively. Furthermore, the degradation temperatures for the BC–MMT composites during this phase were different from that of the pure BC, as shown in Fig. 5. The degradation of pure BC started at 232 °C, which was extended to 260 °C for BC–MMT1 and further increased to 302 and 310 °C for BC–MMT2 and BC–MMT3, respectively. The MMT is thermally stable as the onset of its degradation occurs at a temperature of more than 600 °C (Leszczynska, Njuguna, Pielichowski, & Banerjee, 2007). The incorporation of MMT into the BC matrix during composite preparation is expected to improve the overall thermal stability of BC because its presence inside and on the surface of the BC sheets can protect the cellulose chains against thermal shock. This protection ultimately results in shifting the degradation towards higher temperatures and reduction in the weight loss. Moreover, the hydrogen bonding between the BC and MMT groups may also lead to an improvement in the thermal properties of the BC chains. The improvement in the thermal stability of alkanthiolate self-assembled monolayers by hydrogen bonding has been reported previously (Valiokas, Ostblom, Svedhem, Svensson, & Liedberg, 2002). There was a small difference between the thermal stabilities of the BC–MMT2 and BC–MMT3.

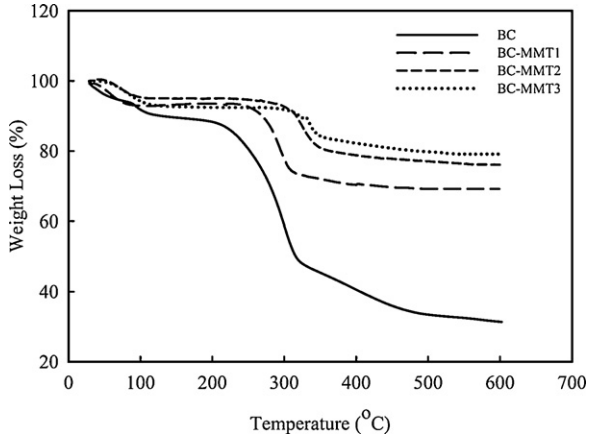

Fig. 5. TGA curves for BC and BC–MMT composites. The composites (BC–MMT1, BC–MMT2 and BC–MMT3) were prepared by impregnation of BC sheets in respective concentrations (1, 2 and 4%) of MMT suspensions at 50 °C and 150 rpm for 24 h.

Table 1
Water holding capacities of the pure BC and BC–MMT composites. The BC–MMT composites (BC–MMT1, BC–MMT2 and BC–MMT3) were prepared by impregnation of BC sheets in respective concentrations (1, 2 and 4%) of MMT suspensions at 150 rpm for 24 h.

Sample	Water holding capacity [g water/g sample]
BC (control)	120.42 (±3.1)
BC–MMT1	83.38 (±2.6)
BC–MMT2	72.39 (±1.9)
BC–MMT3	62.63 (±2.1)

3.6. Mechanical strength

BC is used as a scaffold for tissue engineering and in wound dressing due to its excellent mechanical strength (Li et al., 2011). Structural changes in BC can cause variations in its mechanical properties. Improvements in the mechanical properties of the BC by preparation of its composites with various materials have been reported previously (Phisalaphong et al., 2008; Ul-Islam et al., 2011). Therefore, the intrinsic mechanical properties of the pure BC and the BC–MMT composites were investigated by using a tensile test in order to determine the effects of MMT incorporation on the mechanical strength of BC. Fig. 6A shows the stress–strain curve for the neat BC and the BC–MMT composites, while the results for tensile strength, strain and Young's modulus of the pure BC and the BC–MMT composites are displayed in Fig. 6B.

The results indicated that the maximum tensile strength at the breaking point for all composites was higher than for the pure BC. Similar increases in the tensile properties of the polymer–nanoclay composites have also been reported previously (Liu et al., 2010; Olalekan et al., 2010; Velmurugan & Mohan, 2009). The tensile strength for pure BC was found to be 151.3 MPa, which increased to 191.2 and 209.6 MPa for BC–MMT1 and BC–MMT2, respectively. The tensile strength, however, decreased slightly to 185.0 MPa for BC–MMT3. All the composites exhibited a significant improvement in tensile strength over that of BC. It is well known that MMT particles get attached to the BC network through hydrogen bonding (Darder et al., 2003; Theng, 1970), which strengthens the microfibrils and enhances the overall toughness of the BC. Moreover, the MMT particles incorporated into the BC sheets restrict the mobility of the polymer chains and thus increase the toughness and mechanical strength of the composites (Velmurugan & Mohan, 2009). Similarly, the Young's modulus for BC (4.2 GPa) increased to 6.0, 6.1 and 5.7 GPa for BC–MMT1, BC–MMT2, and BC–MMT3, respectively. It can be observed that the tensile strength and Young's modulus for BC–MMT3 are slightly lower as compared to BC–MMT1 and BC–MMT2, although still higher than those for the pure BC. The relative dry weight of MMT reaches more than 45% of the total weight of BC–MMT3 as shown in Fig. 2. The penetrating particles may disturb the arrangement of micro-fibrils to some extent at such a higher MMT concentration and the shear stress generated at a higher rotation speed (150 rpm), which in turn can affect the tensile strength of the composites. Moreover, agglomeration occurs at high MMT concentration which can result in a decrease in the tensile strength of the composites (Olalekan et al., 2010). The strain of the composite is decreased with the incorporation of MMT particles inside the BC sheets as shown in Fig. 6. The average strain

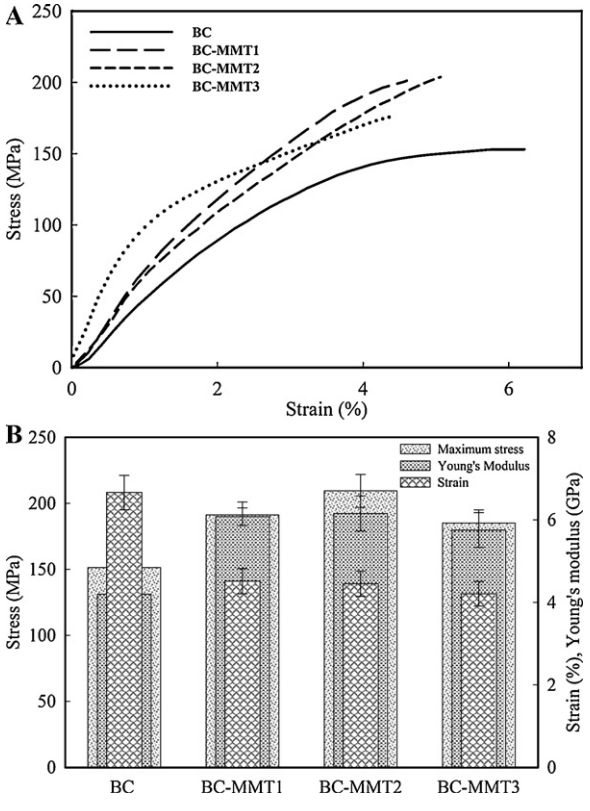

Fig. 6. Mechanical properties of pure BC and BC–MMT composites: (A) stress strain curves; (B) tensile strength at breaking point, strain (%), and Young's modulus. The BC–MMT composites (BC–MMT1, BC–MMT2 and BC–MMT3) were prepared by impregnation of BC sheets in respective concentrations (1, 2 and 4%) of MMT suspensions at 50 °C and 150 rpm for 24 h.

for BC (6.66%) decreased to 4.51%, 4.45% and 4.2% for BC–MMT1, BC–MMT2, and BC–MMT3, respectively. It has been reported that the elasticity of the composite materials decreases with nanoclay incorporation because these can result in fractures of the composite surface and thus the breaking point is attained at a lower strain (Velmurugan & Mohan, 2009). The overall results showed that the mechanical properties of the composites were improved as compared to those of the pure BC by the incorporation of MMT particles, although the properties were lower for BC–MMT3 than for BC–MMT1 and BC–MMT2. This could be an important driving factor for the industrial and biomedical applications of the newly synthesized BC–MMT composites.

3.7. Water holding capacity (WHC) and water release rate (WRR)

Modern wound healing processes focus on keeping the wound moist for a long time because a moist environment increases the penetration of active substances and enable an easy and painless dressing change without damage to the newly formed skin (Shezad et al., 2010; Ul-Islam et al., 2011). BC has been extensively used as a wound dressing material due to its high water holding capability and slow water release rate (Shezad et al., 2010; Ul-Islam et al., 2011). However, these properties of BC are usually modified by altering the structural features or by incorporating additional substances into the BC for the preparation of its composites (Ul-Islam et al., 2011; Zhang & Luo, 2011). Therefore, WHCs of the pure BC and the newly prepared BC–MMT composites were investigated. The overall results (Table 1) revealed that the WHCs of the composites were lower than that of the pure BC. Moreover, the WHC decreased with increasing concentration of MMT in the composites. The WHC of pure BC was 120.42, which decreased to 83.38, 72.39 and 62.63 for BC–MMT1, BC–MMT2, and BC–MMT3, respectively (Table 1). The water molecules are trapped physically at the surface and inside the reticulated BC fibrils (Watanabe, Tabuchi, Morinaga, & Yoshinaga, 1998). When the BC fibrils are loosely arranged, with more empty space between them, then they can trap more water and thus the WHC is high. The deposition of MMT particles on the surface and inside the BC matrix fills the empty pores of BC sheets, as shown in the SEM images of the surfaces and cross sections of the BC–MMT composites (Fig. 1). Moreover, the amount of MMT deposition is increased with increasing MMT concentration, as shown in Fig. 2. The deposition of MMT particles on the surface and in the matrix of BC sheets reduces the empty spaces in BC–MMT composites, which ultimately results in lower water absorption and lower WHC of the composites. MMT adsorption and penetration inside the BC matrix increases with MMT concentration, which in turn results in decreased WHC in the following order, BC > BC–MMT1 > BC–MMT2 > BC–MMT3, as shown in Table 1.

The WRR is of significant importance in biomedical applications of BC (Shezad et al., 2010; Ul-Islam et al., 2011), especially as a wound dressing material. Slow release of water from the BC keeps the wound moist for a longer time. Factors that help to slow down the evaporation of water molecules from the BC surface would further increase its suitability as a dressing material. The WRRs of BC and BC–MMT composites were investigated in order to determine the effect of MMT on the WRR in BC–MMT composites. The results shown in Fig. 7 indicate that the initial water content in pure BC is much higher than that in the composites, but the release of water was drastic, resulting in more than 70% water loss in about 50 h. The water content in pure BC became negligible after 70 h. On the other hand, the initial water contents in all the composites were lower, showing the low WHCs of the composites, but the water released from them more slowly than from the pure BC. More than 50% of the water was still present in the composites after 50 h and the water was almost completely lost only after 90 h. A uniform and slower release of water was observed for the composites, unlike for the

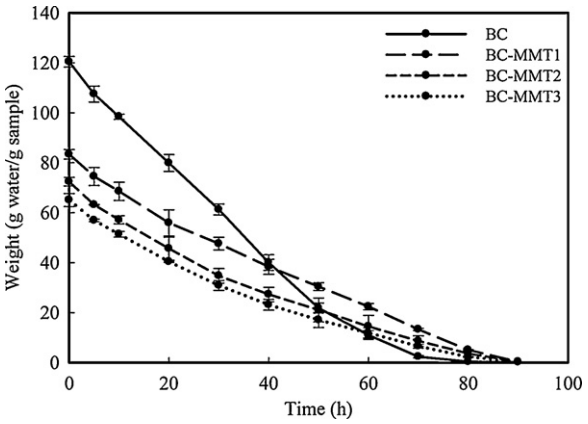

Fig. 7. Water release rates of the pure BC and the BC–MMT composites. The BC–MMT composites (BC–MMT1, BC–MMT2 and BC–MMT3) were prepared by impregnation of BC sheets in respective concentrations (1, 2 and 4%) of MMT suspensions at 50 °C and 150 rpm for 24 h.

pure BC where there was a quick and drastic loss of water throughout. The amount of water retained in a BC–MMT composite is larger than that in BC after 60 h as shown in Fig. 7. The absorbed water molecules were firmly held and protected from evaporation by the MMT particles present on the surfaces of composites although the WHC was lower for composites than for the pure BC. This resulted in retention of the water molecules for a relatively longer time inside the BC sheets. The slow release of water from the composites can be useful in enhancing the biomedical efficacy of BC as a dressing material. Moreover, the MMT has wound healing properties when applied as a wet paste on wounds and skin (Serafica et al., 2002; Ul-Islam et al., 2011). Thus, the MMT in combination with BC in the form of BC–MMT composites as a dressing material can remain wet for a longer time and thus its wound healing capabilities may be further increased.

4. Conclusions

BC–MMT composites were prepared through a simple particle impregnation strategy in order to enhance the physico-mechanical properties of BC. Various analytical techniques including FE-SEM, FTIR and XRD confirmed the formation of the composites. The physico-mechanical and thermal properties of the composites were significantly improved compared to those of pure BC. Moreover, the BC composite also showed improvements in WRR compared to pure BC which is an important feature for BC applications in the medical field. Both MMT and BC have broad applications in biomedical fields and in the present study, the important properties for enhancing their efficacies were combined in the form of the BC–MMT composites.

Acknowledgments

This research was supported by Basic Science Research Program through the National Research Foundation of Korea (NRF) funded by the Ministry of Education, Science and Technology (NRF-2010-0012672). Korea Basic Science Institute (Daegu) is also acknowledged for providing FE-SEM data.

References

Akat, H., Tasdelen, M. A., Du Prez, F., & Yagci, Y. (2008). Synthesis and characterization of polymer/clay nanocomposites by intercalated chain transfer agent. *European Polymer Journal*, *44*, 1949–1954.

Andrei, G., Dima, D., & Andrei, L. (2006). Light weight magnetic composites for aircraft applications. *Journal of Optoelectronics and Advanced Materials*, *8*, 726–730.

Barud, H. S., Rodrigo, T. R., Marques, F. C., Lustri, W. R., Messaddeq, Y., & Ribeiro, S. J. L. (2011). Antimicrobial bacterial cellulose–silver nanoparticles composite membranes. *Journal of Nanomaterials*,. http://dx.doi.org/10.1155/2011/721631

Basavarajappa, S., Arun, K. V., & Davim, J. P. (2009). Effect of filler materials on dry sliding wear behavior of polymer matrix composites – A Taguchi approach. *Journal of Minerals & Materials Characterization & Engineering*, *8*, 379–391.

Bledzki, A. K., & Gassan, J. (1999). Composites reinforced with cellulose based fibres. *Progress in Polymer Science*, *24*, 221–274.

Castro, C., Zuluag, R., Putaux, J., Caro, G., Mondragon, I., & Ganan, P. (2011). Structural characterization of bacterial cellulose produced by *Gluconacetobacter swingsii* sp. from Colombian agroindustrial wastes. *Carbohydrate Polymers*, *84*, 96–102.

Czaja, W., Krystynowicz, A., Bielecki, S., & Brown, R. M. (2006). Microbial cellulose – The natural power to heal wounds. *Biomaterials*, *27*, 145–151.

Darder, M., Colilla, M., & Ruiz-Hitzky, E. (2003). Biopolymer–clay nanocomposites based on chitosan intercalated in montmorillonite. *Chemistry of Materials*, *15*, 3774–3780.

Emami-Razavi, S. H., Esmaeili, N., Forouzannia, S. K., Amanpour, S., Rabbani, S., Alizadeh, A. M., et al. (2006). Effect of bentonite on skin wound healing: Experimental study in the rat model. *Acta Medica Iranica*, *44*, 235–240.

Focher, B., Palma, M. T., Canetti, M., Torri, G., Cosentino, C., & Gastaldi, G. (2001). Structural differences between non-wood plant celluloses: Evidence from solid state NMR, vibrational spectroscopy and X-ray diffractometry. *Industrial Crops and Products*, *13*, 193–208.

George, J., Ramana, K. V., Bawa, A. S., & Siddaramaiah. (2011). Bacterial cellulose nanocrystals exhibiting high thermal stability and their polymer nanocomposites. *International Journal of Biological Macromolecules*, *48*, 50–57.

Giannelis, E. P., Krishnamoorti, R., & Manias, E. (1999). Polymer–silicate nanocomposites: Model systems for confined polymers and polymer brushes. *Advances in Polymer Science*, *138*, 107–147.

Gross, R. A., & Kalra, B. (2002). Biodegradable polymers for the environment. *Science*, *297*, 803–807.

Gunister, E., Pestreli, D., Unlu, C. H., Atici, O., & Gungor, N. (2007). Synthesis and characterization of chitosan–MMT biocomposite systems. *Carbohydrate Polymers*, *67*, 358–365.

Gupta, A., Kumar, A., Patnaik, A., & Biswas, S. (2011). Effect of different parameters on mechanical and erosion wear behavior of bamboo fiber reinforced epoxy composites. *International Journal of Polymer Science*,. http://dx.doi.org/10.1155/2011/592906

Haydel, S. E., Remenih, C. M., & Williams, L. B. (2008). Broad-spectrum in vitro antibacterial activities of clay minerals against antibiotic-susceptible and antibiotic resistant bacterial pathogens. *Journal of Antimicrobial Chemotherapy*, *61*, 353–361.

Khan, T., & Park, J. K. (2008). The structure and physical properties of glucuronic acid oligomers produced by a *Gluconacetobacter hansenii* strain using the waste from beer fermentation broth. *Carbohydrate Polymers*, *73*, 438–445.

Leszczyńska, A., Njuguna, J., Pielichowski, K., & Banerjee, J. R. (2007). Polymer/montmorillonite nanocomposites with improved thermal properties. Part I: Factors influencing thermal stability and mechanisms of thermal stability improvement. *Thermochemica Acta*, *453*, 75–96.

Li, S. M., Jia, N., Zhu, J. F., Ma, M. G., & Sun, R. C. (2010). Synthesis of cellulose–calcium silicate nanocomposites in ethanol/water mixed solvents and their characterization. *Carbohydrate Polymers*, *80*, 270–275.

Li, H. X., Kim, S. J., Lee, Y. W., Kee, C. D., & Oh, I. K. (2011). Determination of the stoichiometry and critical oxygen tension in the production culture of bacterial cellulose using saccharified food wastes. *Korean Journal of Chemical Engineering*, *28*, 2306–2311.

Lin, Y. S., & Burggraaf, A. J. (1991). Preparation and characterization of high-temperature thermally stable alumina composite membrane. *Journal of the American Ceramic Society*, *74*, 219–224.

Liu, H., Chaudhary, D., Yusa, S., & Tade, M. O. (2010). Glycerol/starch/Na+–montmorillonite nanocomposites: A XRD, FTIR, DSC and H NMR study. *Carbohydrate Polymers*, *83*, 1591–1597.

Marins, J. A., Soares, B. G., Dahmouche, K., Ribeiro, S. J. L., Barud, H., & Bonemer, D. (2011). Structure and properties of conducting bacterial cellulose–polyaniline nanocomposites. *Cellulose*, *18*, 1285–1294.

Meng, N., Zhou, N. L., Zhang, S. Q., & Shen, J. (2009). Synthesis and antimicrobial activities of polymer/montmorillonite–chlorhexidine acetate nanocomposite films. *Applied Clay Science*, *42*, 667–670.

Netravali, A. N., & Chabba, S. (2003). Composites get greener. *Materials Today*, *6*, 22–29.

Olalekan, S. T., Muyibi, S. A., Shah, Q. H., Alkhatib, M. F., Yusof, F., & Qudsie, I. Y. (2010). Improving the polypropylene–clay composite using carbon nanotubes as secondary filler. *Energy Research Journal*, *1*, 68–72.

Pavlidou, S. (2008). A review on polymer-layered silicates nanocomposites. *Progress in Polymer Science*, *33*, 1119–1198.

Peijs, T. (2002). Composites turn green. *e-Polymers*, *2*, 1–12.

Phisalaphong, M., Suwanmajo, T., & Sangtherapitiku, P. (2008). Novel nanoporous membranes from regenerated bacterial cellulose. *Journal of Applied Polymer Science*, *107*, 292–299.

Ray, S. S., & Okamoto, M. (2003). Polymer/layered silicate nanocomposites: A review from preparation to processing. *Progress in Polymer Science*, *28*, 1539–1641.

Serafica, G., Mormino, R., & Bungay, H. (2002). Inclusion of solid particles in bacterial cellulose. *Applied Microbiology and Biotechnology*, *58*, 756–760.

Seves, A., Testa, G., Bonfatti, A. M., Paglia, E. D., Selli, E., & Marcandalli, B. (2001). Characterization of native cellulose/poly(ethylene glycol) Films. *Macromolecular Materials and Engineering*, *286*, 524–528.

Shah, N., Ha, J. H., & Park, J. K. (2010). Effect of reactor surface on production of bacterial cellulose and water soluble oligosaccharides by *Gluconacetobacter hansenii* PJK. *Biotechnology and Bioprocess Engineering*, *15*, 110–118.

Shezad, O., Khan, S., Khan, T., & Park, J. K. (2010). Physicochemical and mechanical characterization of bacterial cellulose produced with an excellent productivity instatic conditions using a simple fed-batch cultivation strategy. *Carbohydrate Polymers*, *82*, 173–180.

Theng, B. K. G. (1970). Interactions of clay minerals with organic polymers. Some practical applications. *Clays and Clay Minerals*, *18*, 357–362.

Ul-Islam, M., Shah, N., Ha, J. H., & Park, J. K. (2011). Effect of chitosan penetration on physico-chemical and mechanical properties of bacterial cellulose. *Korean Journal of Chemical Engineering*, *28*, 1025–1103.

Valiokas, R., Ostblom, M., Svedhem, S., Svensson, S. C. T., & Liedberg, B. (2002). Thermal stability of self-assembled monolayers: Influence of lateral hydrogen bonding. *The Journal of Physical Chemistry B*, *106*, 10401–10409.

Velmurugan, R., & Mohan, T. P. (2009). Epoxy–clay nanocomposites and hybrids: Synthesis and characterization. *Journal of Reinforced Plastics and Composites*, *28*, 17–37.

Watanabe, K., Tabuchi, M., Morinaga, Y., & Yoshinaga, F. (1998). Structural features and properties of bacterial cellulose produced in agitated culture. *Cellulose*, *5*, 187–200.

Yu, M., Zhang, Q., & Fu, Q. (2004). Preparation and characterization of polyamide 11/clay nanocomposites. *Chinese Journal of Polymer Science*, *22*, 43–47.

Zhang, S., & Luo, J. (2011). Preparation and properties of bacterial cellulose/alginate blend bio-fibers. *Journal of Engineered Fibers and Fabrics*, *6*, 69–72.